Pharmaceutical Research, Vol. 24, No. 2, February 2007 (© 2006)
DOI: 10.1007/s11095-006-9135-x

Research Paper

Kinetic Considerations for the Quantitative Assessment of Efflux Activity and Inhibition: Implications for Understanding and Predicting the Effects of Efflux Inhibition

J. Cory Kalvass[1] and Gary M. Pollack[2,3]

Received November 9, 2005; accepted July 21, 2006; published online December 27, 2006

Purpose. Unexpected and complex experimental observations related to efflux transport have been reported in the literature. This work was conducted to develop relationships for efflux activity (PS_{efflux}) as a function of commonly studied kinetic parameters [permeability-surface area product (PS), efflux ratio (ER), degree of efflux inhibition (ϕ_i), 50% inhibitory concentration (IC_{50}), and Michaelis–Menten constant (K_m)].

Methods. A three-compartment model (apical, cellular, and basolateral) was used to derive flux equations relating the initial rate of flux and steady-state mass transfer in the presence or absence of active efflux. Various definitions of efflux ratio (ER) were examined in terms of permeability-surface area products. The efflux activity (PS_{efflux}) was expressed in terms of ER and PS. The relationships between PS_{efflux} and PS, ER, ϕ_i, IC_{50}, and K_m were solved mathematically. Simulations and examples from the literature were used to illustrate the resulting mathematical relationships.

Results. The relationships derived according to a three-compartment model differed fundamentally from commonly accepted approaches for determining PS_{efflux}, ϕ_i, IC_{50} and K_m. Based on the model assumptions and mathematical derivations, currently used mathematical relationships erroneously imply that efflux activity is proportional to change in PS (i.e., flux or P_{app}) and thus underestimate PS_{efflux} and ϕ_i, and overestimate IC_{50} and K_m.

Conclusions. An understanding of the relationship between efflux inhibition and kinetic parameters is critical for appropriate data interpretation, standardization in calculating and expressing the influence of efflux transport, and predicting the clinical significance of efflux inhibition.

KEY WORDS: absorption; blood–brain barrier; breast cancer resistance protein (BCRP); Caco-2; efflux inhibition; efflux ratio; efflux transporters; MDCK; multidrug resistance; P-glycoprotein; transcellular flux.

[1] Division of Drug Delivery and Disposition, School of Pharmacy, Kerr Hall C.B.# 7360 University of North Carolina at Chapel Hill, Chapel Hill, North Carolina 27599-7360, USA.

[2] Division of Pharmacotherapy and Experimental Therapeutics, School of Pharmacy, Kerr Hall C.B.# 7360 University of North Carolina at Chapel Hill, Chapel Hill, North Carolina 27599-7360, USA.

[3] To whom correspondence should be addressed. (e-mail: gary_pollack@unc.edu)

ABBREVIATIONS: ϕ_i, degree of efflux inhibition; ER_α, asymmetry efflux ratio ($PS_{B\rightarrow A}/PS_{A\rightarrow B}$) or steady-state ($C_A/C_B$); ER_A, apical efflux ratio ($PS_{0,B\rightarrow A}/PS_{B\rightarrow A}$) or steady-state ($C_{A,0}/C_A$); ER_B, basolateral efflux ratio ($PS_{I,A\rightarrow B}/PS_{A\rightarrow B}$) or steady-state ($C_{B,I}/C_B$); ER_C, cellular efflux ratio ($PS_{I,A\rightarrow C}/PS_{A\rightarrow C}$) or steady-state ($C_{C,I}/C_C$); [I], inhibitor concentration; IC_{50}, 50% inhibitory concentration; K_i, inhibitor constant; K_m, Michaelis–Menten constant; PS, observed permeability-surface area product; PS_0, permeability–surface area product in the absence of efflux inhibition; PS_I, permeability–surface area product when efflux is completely inhibited or saturated; passive permeability-surface area product; [S], substrate concentration.

SUBSCRIPTS: A, apical; B, basolateral; C, cellular; app, apparent; max, maximum; I, efflux is completely inhibited or saturated; A→B, apical to basolateral, apical compartment dosed; B→A, basolateral to apical, basolateral compartment dosed; A→C, apical to cellular, apical compartment dosed.

INTRODUCTION

Xenobiotic efflux transporters such as P-glycoprotein (P-gp) can influence drug disposition, efficacy, and safety. Inhibition of efflux transporters may have beneficial (e.g., increased absorption, enhanced presentation to the target site) or adverse (e.g., unexpected or dangerous drug interactions) effects (1). Specific efflux inhibitors are in development to increase oral bioavailability, to target therapeutics to the central nervous system (CNS), and to reverse multidrug resistance (MDR) in cancer (2–4). In addition, drug–drug interactions at the level of efflux transporters have been identified and represent an area of increasing interest (5–7).

Various *in vitro* and *in vivo* models have been developed to identify substrates and inhibitors of efflux transporters and to predict the effects of efflux inhibition on drug disposition and action. These models include cell monolayers (Caco-2 and transfected MDCKII cells), perfused organs (brain, liver, kidney, and intestine), and intact animals (transporter-deficient animals [e.g., mdr1a/b deficient mice]; coadministration of efflux inhibitors *in vivo*) (8–11). The predictive utility of these models depends on accurate determination of efflux activity (PS_{efflux}), substrate affinity (K_m), inhibitor potency (IC_{50}), and the degree of efflux inhibition (ϕ_i). Unfortunately, the relationships between PS_{efflux} and these other experimental parameters are poorly understood, leading to data misinterpretation and inaccurate *in vitro–in vivo* predictions.

Several experimental strategies comprised of different designs and data analysis methods have been used to study apical efflux. Often, an observation in one experimental system is used to predict behavior in another system. For example, Caco-2 monolayer flux studies are used to make predictions of intestinal drug absorption in humans. Kinetic, molecular, and computational models are proposed to provide a better understanding of experimental observations and to make predictions of system behavior. Various types of models with differing degrees of complexity have been proposed for apical efflux (8–14). Even though the models differ in complexity and details, most share some common elements: distinct apical, basolateral, and cellular compartments, with efflux transport located on the apical membrane. A comprehensive understanding of system behavior for the most basic model structure, one that incorporates the fewest assumptions, is an important first step in critically evaluating the kinetic consequences of efflux transport.

In the present work, a simple kinetic model based on the prototypical efflux transporter P-gp was constructed and used to derive the theoretical relationships between PS_{efflux} and experimental parameters (K_m, IC_{50}, and ϕ_i). The resulting mathematical relationships were compared to commonly accepted approaches for calculating PS_{efflux}, ϕ_i, K_m, and IC_{50}. Kinetic considerations suggest that commonly used relationships for determining the experimental parameters PS_{efflux}, K_m, and IC_{50} may be confounded by the efflux activity of the model system as well as the choice of substrate.

THEORETICAL

The simplest kinetic model consistent with efflux attenuating initial rate of apical-to-basolateral (A-to-B) flux is a three-compartment system (Fig. 1) in which PS_A and PS_B represent the passive permeability-surface area product of the apical and basolateral membrane, respectively, and PS_{efflux} represents the permeability-surface area product due to efflux transport. This scheme has been used to represent apical efflux (8,14) and is capable of representing the *in vitro* and *in vivo* models used to study the impact of efflux transporters (Table I). The kinetic model associated with this scheme can be described by the following set of differential equations:

$$\frac{dX_A}{dt} = C_C(PS_A + PS_{efflux}) - C_A PS_A \quad (1\text{–}1)$$

$$\frac{dX_C}{dt} = C_A PS_A + C_B PS_B - C_C(PS_A + PS_B + PS_{efflux}) \quad (1\text{–}2)$$

$$\frac{dX_B}{dt} = C_C PS_B - C_B PS_B \quad (1\text{–}3)$$

where dX_A/dt, dX_B/dt and dX_C/dt represent the substrate flux into and out of the apical, basolateral, and cellular compartments, respectively; C_A, C_B, and C_C represent substrate concentration in each compartment; PS_A and PS_B represent the passive permeability-surface area product of the apical and basolateral membranes; and PS_{efflux} represents the permeability-surface area product of efflux activity. When substrate concentrations approach or exceed the K_m for the efflux transport protein:

$$PS_{efflux} = \frac{PS_{efflux,max}}{C_C + K_m} \quad (1\text{–}4)$$

where $PS_{efflux,max}$ equals maximal efflux activity.

Initial Rate of B-to-A Flux in the Presence or Absence of Active Efflux

Assuming initial unidirectional flux into the apical compartment (i.e., $X_A = 0$) and rapid equilibration between the basolateral and cellular compartments ($dX_C/dt = 0$), the flux in the B-to-A direction and the concentration in the cellular compartment (C_C) can be described by Eqs. (2–1) and (2–2), respectively.

$$\frac{dX_A}{dt} = C_C(PS_A + PS_{efflux}) \quad (2\text{–}1)$$

$$C_C = \frac{C_B PS_B}{(PS_A + PS_B + PS_{efflux})} \quad (2\text{–}2)$$

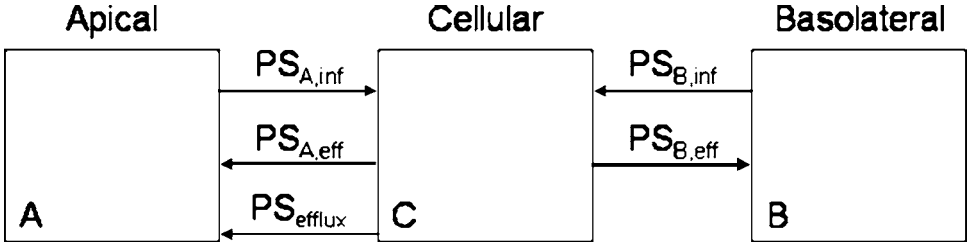

Fig. 1. Three-compartment model consistent with efflux attenuating the initial rate of flux in the A-to-B direction. $PS_{A,inf}$ and $PS_{A,eff}$, represent the passive permeability–surface area product of the apical membrane, whereas, $PS_{B,inf}$ and $PS_{B,eff}$ represent the passive permeability–surface area products of the basolateral membrane. PS_{efflux} represents the permeability–surface area product of efflux activity. It is assumed $PS_{A,inf} = PS_{A,eff} = PS_A$ and $PS_{B,inf} = PS_{B,eff} = PS_B$.

Substitution of Eq. (2–2) into Eq. (2–1) yields the B-to-A flux equation:

$$\frac{dX_{A,B\rightarrow A}}{dt} = \frac{C_B \times PS_B \times (PS_A + PS_{efflux})}{PS_A + PS_B + PS_{efflux}} \quad (2\text{–}3)$$

In the absence of efflux ($PS_{efflux} = 0$), the flux in the B-to-A direction is given by:

$$\frac{dX^{w/o\ efflux}_{A,B\rightarrow A}}{dt} = \frac{C_B \times PS_B \times PS_A}{PS_A + PS_B} \quad (2\text{–}4)$$

Initial Rate of A-to-B Flux in the Presence or Absence of Active Efflux

Assuming initial unidirectional flux into the basolateral compartment (i.e., $X_B = 0$) and rapid equilibration between the apical and cellular compartments ($dX_C/dt = 0$), the flux in the A-to-B direction and the concentration in the cellular compartment (C_C) can be described by Eqs. (3–1) and (3–2), respectively:

$$\frac{dX_B}{dt} = C_C PS_B \quad (3\text{–}1)$$

$$C_C = \frac{C_A PS_A}{(PS_A + PS_B + PS_{efflux})} \quad (3\text{–}2)$$

Substitution of Eq. (3–2) into Eq. (3–1) yields the A-to-B flux equation:

$$\frac{dX_{B,A\rightarrow B}}{dt} = \frac{C_A \times PS_A \times PS_B}{PS_A + PS_B + PS_{efflux}} \quad (3\text{–}3)$$

In the absence of efflux ($PS_{efflux} = 0$), A-to-B flux is given by Eq. (3–4):

$$\frac{dX^{w/o\ efflux}_{B,A\rightarrow B}}{dt} = \frac{C_A \times PS_A \times PS_B}{PS_A + PS_B} \quad (3\text{–}4)$$

Initial Rate of Cellular Influx

Assuming initial unidirectional uptake into the cellular compartment (i.e., $X_C = 0$), flux into the cellular compartment (C_C) can be described by Eqs. (4–1) and (4–2) following administration into the apical and basolateral compartments, respectively:

$$\frac{dX_C}{dt} = C_A PS_A \quad (4\text{–}1)$$

$$\frac{dX_C}{dt} = C_B PS_B \quad (4\text{–}2)$$

Table I. Apical, Cellular, and Basolateral Compartments of Various Model Systems

Model system	Apical	Cellular	Basolateral	Relevant ER[a]
Cell monolayer	Apical chamber	Cell monolayer	Basolateral chamber	ER_A—absorption ER_B—secretion ER_α—intracellular concentration
Calcein-AM assay	Extracellular space	Intracellular space	N/A	ER_A—not applicable ER_B—not applicable ER_α—intracellular concentration
MDR cell	Extracellular space	Intracellular space	N/A	ER_A—not applicable ER_B—not applicable ER_α—intracellular concentration
MDR cell	Extracellular space	Cellular membrane	Intracellular space	ER_A—efflux from intracellular space ER_B—uptake into intracellular space ER_α—membrane concentration
Intestine	GI lumen	Epithelial cell	Blood	ER_A—intestinal absorption ER_B—intestinal secretion ER_α—intracellular concentration
Kidney	Tubule lumen (urine)	Tubule epithelial cell	Blood	ER_A—not applicable ER_B—renal secretion ER_α—intracellular concentration
Liver	Canalicular space (bile)	Hepatocyte	Blood	ER_A—not applicable ER_B—secretion from blood to bile ER_α—hepatocyte intracellular concentration
Blood–brain barrier	Capillary lumen (blood)	Endothelial cell	Brain	ER_A—brain uptake ER_B—brain efflux ER_α—brain-to-plasma ratio

[a] Relevant efflux ratio for each experimental system.

Steady-State Concentrations in Compartments A, B, and C

The steady-state substrate concentration in compartments A, B, and C can be determined by solving differential Eqs. (1–1), (1–2), and (1–3) for concentration at infinite time after administration of mass X_0 to the system:

$$C_{A(t=\infty)} = \frac{X_{A(t=\infty)}}{V_A} = \frac{X_0(PS_A + PS_{efflux})}{(PS_{efflux} \times V_A) + PS_A(V_A + V_B + V_C)} \quad (5\text{–}1)$$

$$C_{B(t=\infty)} = \frac{X_{B(t=\infty)}}{V_B} = \frac{X_0 \times PS_A}{(PS_{efflux} \times V_A) + PS_A(V_A + V_B + V_C)} \quad (5\text{–}2)$$

$$C_{C(t=\infty)} = \frac{X_{C(t=\infty)}}{V_C} = \frac{X_0 \times PS_A}{(PS_{efflux} \times V_A) + PS_A(V_A + V_B + V_C)} \quad (5\text{–}3)$$

In the absence of active efflux, the steady-state concentrations in compartments A, B, and C are equivalent, and may be expressed as:

$$C_{(t=\infty)}^{w/o\ efflux} = \frac{X_0}{(V_A + V_B + V_C)} \quad (5\text{–}4)$$

Definition of Basolateral Efflux Ratio and Efflux Activity

The basolateral efflux ratio (ER_B) can be defined as the ratio of the initial rate of flux in the A-to-B direction when efflux is inhibited completely [Eq. (3–4)] divided by the initial rate of flux in the A-to-B direction when efflux is not inhibited [Eq. (3–3)]:

$$ER_B = \frac{\frac{dX_{B,A\rightarrow B}^{w/o\ efflux}}{dt}}{\frac{dX_{B,A\rightarrow B}}{dt}} = \frac{PS_A + PS_B + PS_{efflux}}{PS_A + PS_B} \quad (6\text{–}1)$$

Alternatively, ER_B can be defined as the steady-state concentration in the basolateral compartment when efflux is inhibited completely [Eq. (5–4)] divided by the steady-state concentration in the basolateral compartment when efflux is not inhibited [Eq. (5–2)]:

$$ER_{B(t\rightarrow\infty)} = \frac{C_B^{w/o\ efflux}}{C_B} = 1 + \frac{PS_{efflux} \times V_A}{PS_A(V_A + V_B + V_C)} \quad (6\text{–}2)$$

Efflux activity (PS_{efflux}) can be expressed in terms of ER_B by rearrangement of Eqs. (6–1) and (6–2):

$$PS_{efflux} = (PS_A + PS_B)(ER_B - 1) \quad (6\text{–}3)$$

$$PS_{efflux} = \frac{(V_A + V_B + V_C)}{V_A} PS_A\left(ER_{B(t\rightarrow\infty)} - 1\right) \quad (6\text{–}4)$$

Definition of Asymmetry Efflux Ratio and Efflux Activity

Assuming that donor concentrations are identical (C_A=C_B), the asymmetry efflux ratio (ER_α) can be defined as the ratio of the initial rate of flux in the B-to-A direction [Eq. (2–3)] divided by the initial rate of flux in the A–to–B direction [Eq. (3–3)]:

$$ER_\alpha = \frac{\frac{dX_{A,B\rightarrow A}}{dt}}{\frac{dX_{B,A\rightarrow B}}{dt}} = \frac{PS_A + PS_{efflux}}{PS_A} \quad (7\text{–}1)$$

Alternatively, ER_α can be defined as the apical steady-state concentration [Eq. (5–1)] divided by the steady-state concentration in the basolateral compartment [Eq. (5–2)]:

$$ER_{\alpha(t\rightarrow\infty)} = \frac{C_A}{C_B} = \frac{PS_A + PS_{efflux}}{PS_A} \quad (7\text{–}2)$$

Efflux activity (PS_{efflux}) then can be solved in terms of ER_α as:

$$PS_{efflux} = PS_A(ER_\alpha - 1) \quad (7\text{–}3)$$

$$PS_{efflux} = PS_A\left(ER_{\alpha(t\rightarrow\infty)} - 1\right) \quad (7\text{–}4)$$

Definition of Cellular Efflux Ratio and Efflux Activity

The cellular efflux ratio (ER_C) can be defined as the ratio of the initial rate of flux in the A-to-C direction when efflux is inhibited completely [Eq. (4–1)] divided by the initial rate of flux in the A-to-C direction when efflux is not inhibited [Eq. (4–1)]:

$$ER_C = \frac{\frac{dX_{C,A\rightarrow C}^{w/o\ efflux}}{dt}}{\frac{dX_{C,A\rightarrow C}}{dt}} = 1 \quad (8\text{–}1)$$

ER_C also can be defined as the steady-state concentration in the cellular compartment when efflux is inhibited completely [Eq. (5–4)] divided by the steady-state concentration in the cellular compartment when efflux is not inhibited [Eq. (5–3)]:

$$ER_{C(t\rightarrow\infty)} = \frac{C_C^{w/o\ efflux}}{C_C} = 1 + \frac{PS_{efflux} \times V_A}{PS_A(V_A + V_B + V_C)} \quad (8\text{–}2)$$

Efflux activity (PS_{efflux}) can be expressed in terms of ER_C as:

$$PS_{efflux} = \frac{(V_A + V_B + V_C)}{V_A} PS_A\left(ER_{C(t\rightarrow\infty)} - 1\right) \quad (8\text{–}3)$$

Definition of Apical Efflux Ratio and Efflux Activity

The apical efflux ratio (ER_A) can be defined as the ratio of the initial rate of flux in the B-to-A direction when efflux

is not inhibited [Eq. (2–3)] divided by the initial rate of flux in the B-to-A direction when efflux is inhibited completely [Eq. (2–4)]:

$$ER_A = \frac{\frac{dX_{A,B\to A}}{dt}}{\frac{dX^{w/o\ efflux}_{A,B\to A}}{dt}} = \frac{(PS_A + PS_B)(PS_A + PS_{efflux})}{PS_A(PS_A + PS_B + PS_{efflux})} \leq \frac{(PS_A + PS_B)}{PS_A} \quad (9\text{–}1)$$

Alternatively, ER_A can be defined as the steady-state concentration in the apical compartment when efflux is not inhibited [Eq. (5–1)] divided by the observed steady-state concentration in the apical compartment when efflux is inhibited completely [Eq. (5–4)]:

$$ER_{A(t\to\infty)} = \frac{C_A}{C_A^{w/o\ efflux}} = \frac{(PS_A + PS_{efflux})(V_A + V_B + V_C)}{(PS_{efflux} \times V_A) + PS_A(V_A + V_B + V_C)} \leq \frac{V_A + V_B + V_C}{V_A} \quad (9\text{–}2)$$

Efflux activity (PS_{efflux}) then can be expressed in terms of ER_A as:

$$PS_{efflux} = \frac{(PS_A + PS_B)PS_A(ER_A - 1)}{(PS_A + PS_B) - (PS_A \times ER_A)} \quad (9\text{–}3)$$

$$PS_{efflux} = \frac{(V_A + V_B + V_C)PS_A(ER_A - 1)}{(V_A + V_B + V_C) - (V_A \times ER_A)} \quad (9\text{–}4)$$

RESULTS AND DISCUSSION

Efflux Activity is Proportional to the Quantity ER-1, not to Attenuation or Enhancement of Flux

The mathematical relationships derived from the three-compartment model in Fig. 1 indicate that efflux attenuates flux in the A-to-B direction and enhances flux in the B-to-A direction. However, neither the attenuation of flux in the A-to-B nor the enhancement of flux in the B-to-A direction is proportional to the efflux activity (PS_{efflux}) [Eqs. (2–3) and (3–3); illustrated in Fig. 2]. In contrast, according to the three-compartment model [Table II; illustrated in Fig. 3; and Eqs. (6–3), (6–4), (7–3), (7–4), and (8–3)], PS_{efflux} is proportional to ER_B-1, ER_α-1, and ER_C-1. The fact that PS_{efflux} is not proportional to flux but is proportional to ER_B-1, ER_α-1, and ER_C-1 has important implications regarding the calculation of PS_{efflux}, K_m, and IC_{50}.

Numerous approaches with little consensus have been proposed to calculate and express PS_{efflux} (Table III). Often, PS_{efflux} is calculated directly from the magnitude of attenuation or enhancement in flux caused by efflux. Since the magnitude of attenuation and enhancement in flux is not proportional to PS_{efflux}, and therefore should not be used to calculate PS_{efflux} directly, we propose a novel method, consistent with the simple three-compartment model for calculating and expressing PS_{efflux}.

From previous mathematical derivations, PS_{efflux} can be defined in terms of PS_A, PS_B, and efflux ratios (Table II), and is proportional to ER_α-1, ER_B-1, and $ER_{C(t\to\infty)}$-1 (Table II; illustrated in Fig. 3). However, in most experimental designs, PS_A and PS_B are not determined, but the passive permeability-surface area product in the A-to-B direction ($PS_{I,A\to B}$) is measured. The $PS_{I,A\to B}$ can be expressed in terms of PS_A and PS_B as follows:

$$PS_{I,A\to B} = \frac{PS_A \times PS_B}{PS_A + PS_B} \quad (10\text{–}1)$$

If PS_A and PS_B are assumed to be equal, rearrangement of Eq. (10–1) indicates that PS_A and PS_B equal $2PS_{I,A\to B}$. PS_{efflux} can be expressed in terms of $PS_{I,A\to B}$ and ER by substituting $2PS_{I,A\to B}$ for PS_A and PS_B into Eqs. (6–3), (7–3), and (8–3), yielding Eqs. (10–2), (10–3), and (10–4) respectively:

$$PS_{efflux} = 4PS_{I,A\to B}(ER_B - 1) \quad (10\text{–}2)$$

$$PS_{efflux} = 2PS_{I,A\to B}(ER_\alpha - 1) \quad (10\text{–}3)$$

$$PS_{efflux} = 2PS_{I,A\to B}\frac{(V_A + V_B + V_C)}{V_A}\left(ER_{C(t\to\infty)} - 1\right) \quad (10\text{–}4)$$

From the preceding equations, the precise value of PS_{efflux} can be expressed in terms of commonly obtained experimental parameters, namely efflux ratio and passive permeability. In qualitative terms, PS_{efflux} is proportional to ER-1 multiplied by the passive permeability. This relationship differs from other commonly cited approaches for expressing PS_{efflux}; however, it is kinetically sound (based on the inherent assumptions of the model in Fig. 1), and it is intuitive in that the efflux ratio of a substrate is dependent on both efflux activity and the substrate passive permeability. Expressing PS_{efflux} in terms of $PS_{I,A\to B}$ and ER also is convenient, and allows for precise quantitation and comparison of PS_{efflux} between different substrates, model systems, and laboratories.

As in the case for PS_{efflux}, flux should not be used to directly calculate K_m or IC_{50}. This is true because, when determining K_m or IC_{50}, it is necessary to relate substrate or inhibitor concentrations to the value PS_{efflux} and because flux is not proportional to PS_{efflux}. Instead of using flux, K_m and IC_{50} may be calculated directly from ER_α-1, ER_B-1, and $ER_{C(t\to\infty)}$-1 since ER-1 is proportional to PS_{efflux}. The difference between calculating IC_{50} directly from P_{app} *versus* ER-1 can be illustrated with a recent example from the literature. Although numerous relevant data sets can be found in the literature, a data set from Chen *et al*. (2002) was chosen due to the high quality of the data and the extensive characterization of the Michaelis–Menten profile (Fig. 4) (15). The conclusions drawn from consideration of this experimental data set are generalizable to other situations. Briefly, the investigators used an *in situ* rat brain perfusion technique to examine the ability of the P-gp inhibitor GF-120918 to inhibit the P-gp-mediated efflux of quinidine.

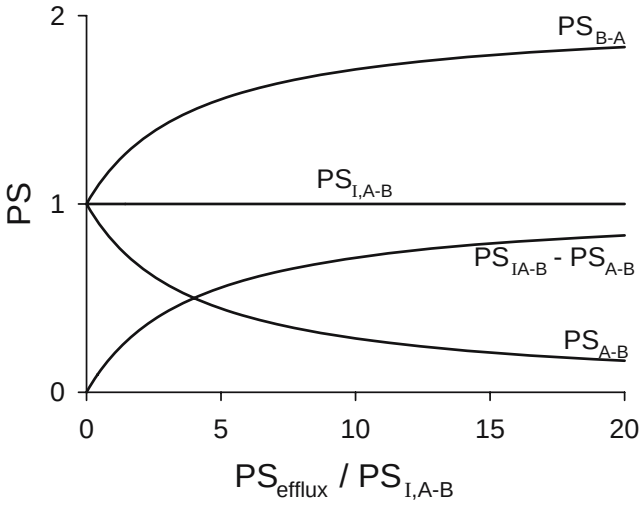

Fig. 2. Relationship between efflux activity (PS_{efflux}) and permeability–surface area product (PS). Efflux activity was normalized for the A-to-B passive permeability–surface area product ($PS_{I,A\text{-}B}$). PS_A and PS_B were assumed to be equal, therefore $PS_{I,A\text{-}B}$=1/2 PS_A. Since P_{app} and flux are proportional to PS, substituting P_{app} or flux for PS will yield the identical relationship.

Various concentrations of GF-120918 were examined; as concentrations of GF-120918 were increased, the P_{app} value for quinidine increased to a plateau at ~13-fold. In such experiments, the $IC_{50,app}$ of the inhibitor often is calculated by fitting a modified Michaelis–Menten equation to the P_{app} *vs*. inhibitor concentration data. In order to illustrate why $IC_{50,app}$ should not be calculated in this manner, we used a modified Michaelis–Menten equation to calculate both the $IC_{50,app}$ (from the P_{app} and GF-120918 concentration data) and the "true" IC_{50} (from ER and GF-120918 data). Even though the same experimental data were used in calculating $IC_{50,app}$ and $IC_{50,}$ the $IC_{50,app}$ (0.56 μM) was 13-fold higher than the IC_{50} (0.042 μM). It is clear that the $IC_{50,app}$ calculated from P_{app} data differs fundamentally from the IC_{50} calculated from ER data. Since changes in P_{app} are not proportional to changes in PS_{efflux}, IC_{50} and K_m should not be calculated by fitting a modified Michaelis–Menten equation to P_{app} data. Mathematical treatment of IC_{50} and K_m will be explored in further detail in a later section; at this point, we simply demonstrate that calculating IC_{50} or K_m from flux or P_{app} values is not equivalent to calculations based on ER values.

B-to-A Flux (Secretory Flux) Is Minimally Sensitive to Efflux Activity

Apical efflux clearly enhances flux in the B-to-A direction. However, this enhancement is not proportional to either efflux activity (PS_{efflux}) or ER_A-1 [Eqs. (2–3) and (9–1); illustrated in Figs. 2 and 3]. The fold increase in the B-to-A flux is given by the ER_A in Eq. (9–1):

$$ER_A = \frac{\frac{dX_{A,B\to A}}{dt}}{\frac{dX^{w/o\ efflux}_{A,B\to A}}{dt}} = \frac{(PS_A + PS_B)(PS_A + PS_{efflux})}{PS_A(PS_A + PS_B + PS_{efflux})} \leq \frac{(PS_A + PS_B)}{PS_A} \quad (9\text{–}1)$$

Taking into account the model assumptions discussed previously, the maximum value of ER_A is $(PS_A + PS_B)/PS_A$ (i.e., 2, assuming PS_A=PS_B). In other words, if passive permeabilities across the apical and basolateral membranes are similar, then the maximum increase in B-to-A flux that efflux can cause is twofold. Therefore, measuring the effect of efflux on permeability in the B-to-A direction is uninformative, as flux in the B-to-A direction is not proportional to, and is in fact minimally sensitive to, PS_{efflux}.

Experimental evidence is consistent with this predicted behavior. For example, the B-to-A flux of loperamide, amprenavir, and eletriptan in MDR1-transfected MDCK cell monolayers increased only 1.5- to 2.1-fold despite a 10-, 29-,

Table II. Relationships Between Efflux Ratio, Permeability–Surface Area Products, and Efflux Activity

Definition of efflux ratio	Assumptions	Efflux activity
$ER_B = \frac{\frac{dX^{w/o\ efflux}_{B,A\to B}}{dt}}{\frac{dX_{B,A\to B}}{dt}} = \frac{PS_A+PS_B+PS_{efflux}}{PS_A+PS_B}$	Initial uptake rate (i.e., X_B=0); rapid equilibrium between A and C	$PS_{efflux} = (PS_A + PS_B)(ER_B - 1)$
$ER_{B(t\to\infty)} = \frac{C^{w/o\ efflux}_B}{C_B} = 1 + \frac{PS_{efflux}\times V_A}{PS_A(V_A+V_B+V_C)}$	None	$PS_{efflux} = \frac{(V_A+V_B+V_C)}{V_A} PS_A(ER_B - 1)$
$ER_\alpha = \frac{\frac{dX_{A,B\to A}}{dt}}{\frac{dX_{B,A\to B}}{dt}} = \frac{PS_A+PS_{efflux}}{PS_A}$	Initial uptake rate (i.e., X_A=0); rapid equilibrium between B and C initial uptake rate (i.e., X_B=0); rapid equilibrium between A and C	$PS_{efflux} = PS_A(ER_\alpha - 1)$
$ER_{\alpha(\tau\to\infty)} = \frac{C_A}{C_B} = \frac{PS_A+PS_{efflux}}{PS_A}$	None	$PS_{efflux} = PS_A(ER_\alpha - 1)$
$ER_C = \frac{\frac{dX^{w/o\ efflux}_{C,A\to C}}{dt}}{\frac{dX_{C,A\to C}}{dt}} = 1$	Initial uptake rate (i.e., X_C=0);	n/a
$ER_{C(t\to\infty)} = \frac{C^{w/o\ efflux}_e}{C_C} = 1 + \frac{PS_{efflux}\times V_A}{PS_A(V_A+V_B+V_C)}$	None	$PS_{efflux} = \frac{(V_A+V_B+V_C)}{V_A} PS_A(ER_C - 1)$
$ER_A = \frac{\frac{dX_{A,B\to A}}{dt}}{\frac{dX^{w/o\ efflux}_{A,B\to A}}{dt}} = \frac{(PS_A+PS_B)(PS_A+PS_{efflux})}{PS_A(PS_A+PS_B+PS_{efflux})} \leq \frac{(PS_A+PS_B)}{PS_A}$	Initial uptake rate (i.e., X_A=0); rapid equilibrium between B and C	$PS_{efflux} = \frac{(PS_A+PS_B)PS_A(ER_A-1)}{(PS_A+PS_B)-(PS_A\times ER_A)}$
$ER_{A(t\to\infty)} = \frac{C_A}{C^{w/o\ efflux}_A} = \frac{(PS_A+PS_{efflux})(V_A+V_B+V_C)}{(PS_{efflux}\times V_A)+PS_A(V_A+V_B+V_C)} \leq \frac{V_A+V_B+V_C}{V_A}$	None	$PS_{efflux} = \frac{(V_A+V_B+V_C)PS_A(ER_A-1)}{(V_A+V_B+V_C)-(V_A\times ER_A)}$

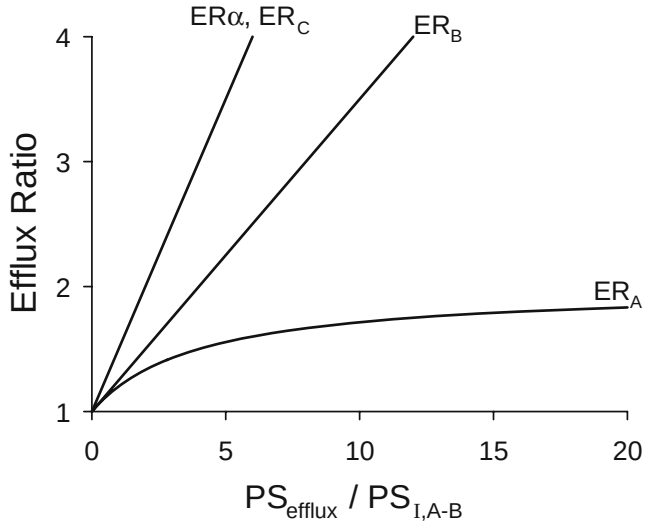

Fig. 3. Relationship between efflux activity (PS_{efflux}) and asymmetry (ER_α), absorptive (ER_B), secretory (ER_A), or intracellular (ER_C) efflux ratio. Efflux activity was normalized for the A-to-B passive permeability surface area product ($PS_{I,A\text{-}B}$). PS_A and PS_B were assumed to be equal, therefore $PS_{I,A\text{-}B} = 1/2\ PS_A$.

and 45-fold decrease in A-to-B flux, respectively (16). Another experimental observation consistent with a maximum twofold increase in B-to-A flux is the influence of P-gp-mediated efflux on the equilibration half-life of fentanyl, alfentanil, methadone, loperamide across the blood–brain barrier (BBB). These opioids were used as *in vivo* probes in P-gp-competent and P-gp-deficient mice to assess the influence of P-gp-mediated efflux on brain-to-plasma ratio ($K_{p,brain}$) and the pseudo-first-order rate constant governing the time-dependent approach of the brain-to-plasma ratio to its equilibrium value ($K_{eq,brain}$). Based on the principle that $K_{eq,brain}$ is influenced only by the rate of egress from brain, $K_{eq,brain}$ should be directly proportional to $PS_{B\rightarrow A}$. Thus, the fold change in $K_{eq,brain}$ can be expressed in terms of ER_A. In contrast, the fold change in brain-to-plasma ratio can be expressed in terms ER_α. So by studying the effect of P-gp-mediated efflux on $K_{p,brain}$ and $K_{eq,brain}$, the influence of efflux on the ER_α and ER_A can be deduced *in vivo*. P-gp-mediated efflux had a more pronounced effect on the brain-to-plasma ratio (1.9- to 44-fold change) than on the brain equilibration half-life (1.0- to 2.4-fold change). Without examining the experimental observations in terms of ER_A and ER_α, the experimental observations in $K_{eq,brain}$ may be difficult to rationalize. However, the results are precisely what would be expected based on the model and associated assumptions (Table IV).

Despite the kinetic considerations, for some substrates apical efflux transport increases flux in the B-to-A direction by more than twofold. For example, in Caco-2 monolayers the efflux transporter P-gp had a pronounced effect (tenfold) on the B-to-A flux of rhodamine 123, even though P-gp efflux minimally attenuated rhodamine 123 flux in the A-to-B direction (17). In the same Caco-2 studies, rhodamine 123 had low membrane permeability, with A-to-B flux occurring primarily by the paracellular route. However, the B-to-A flux was much higher than the A-to-B flux, and it occurred via the transcellular route, because rhodamine 123 was transported across the basolateral membrane by active uptake. Active uptake of rhodamine 123 across the basolateral membrane violates the assumptions of the basic kinetic model ($PS_{B,inf} \neq PS_{B,eff}$). Therefore, efflux has a more pronounced effect on B-to-A flux than the kinetic scheme would suggest.

Table III. Comparison of Methods for the Calculation of Experimental Parameters

Parameter	Method(s) from literature	Method(s) derived from kinetic theory
IC_{50}	$PS = PS_0 + (PS_I - PS_0) \times \frac{[I]}{[I]+IC_{50,app}}$ (27)	$PS = \frac{PS_I \times PS_0}{PS_I + (PS_0 - PS_I) \times \frac{[I]}{[I]+IC_{50}}}$
		$ER - 1 = \left(\frac{PS_I}{PS_0} - 1\right) \frac{IC_{50}}{[I]+IC_{50}}$
K_m	$PS = PS_0 + (PS_I - PS_0) \times \frac{[S]}{[S]+K_{m,app}}$ (28,29)	$PS = \frac{PS_I \times PS_0}{PS_I + (PS_0 - PS_I) \times \frac{[S]}{[S]+K_m}}$
		$ER - 1 = \left(\frac{PS_I}{PS_0} - 1\right) \frac{K_m}{[S]+K_m}$
ϕ_i	$\phi_{i,app} = \frac{PS - PS_0}{PS_I - PS_0}$ (30)	$\phi_i = \frac{ER_{max} - ER}{ER_{max} - 1}$
		$\phi_i = \frac{PS_I}{PS} \times \frac{(PS - PS_0)}{(PS_I - PS_0)}$
	$\phi_{i,app} = 1 - \frac{PS_{,B\rightarrow A} - PS_{,A\rightarrow B}}{PS_{0,B\rightarrow A} - PS_{0,A\rightarrow B}}$ (31)	$\phi_i = \frac{PS_{I,A\rightarrow B}}{PS_{,A\rightarrow B}} \times \left(1 - \frac{PS_{B\rightarrow A} - PS_{A\rightarrow B}}{PS_{0,B\rightarrow A} - PS_{0,A\rightarrow B}}\right)$
		$\phi_i \geq 1 - \frac{1}{\text{fold}\,\Delta PS}$ [a]
PS_{efflux}	$PS_{efflux,app} = PS_I\text{-}PS$ $PS_{efflux,app} \propto PS_I\text{-}PS$ $PS_{efflux,app} \propto ER_B$ $PS_{efflux,app} \propto ER_C$ $PS_{efflux,app} \propto ER_\alpha$	$PS_{efflux} = 4PS_{I,A\rightarrow B}(ER_B - 1)$ $PS_{efflux} = 2PS_{I,A\rightarrow B}(ER_\alpha - 1)$ $PS_{efflux} \propto PS_{I,A\rightarrow B}(ER - 1)$
$K_{m,app}$	$K_{m,app} = K_{m,app}$	$K_{m,app} = K_m \times ER_{max}$
$IC_{50,app}$	$IC_{50,app} = IC_{50,app}$	$IC_{50,app} = IC_{50} \times ER_{max}$

Note: Since flux and P_{app} are proportional to PS, flux and P_{app} can be substituted for PS ER = ER_B, ER_C, or ER_α.
[a] Rearrangement of Eq. (12-10).

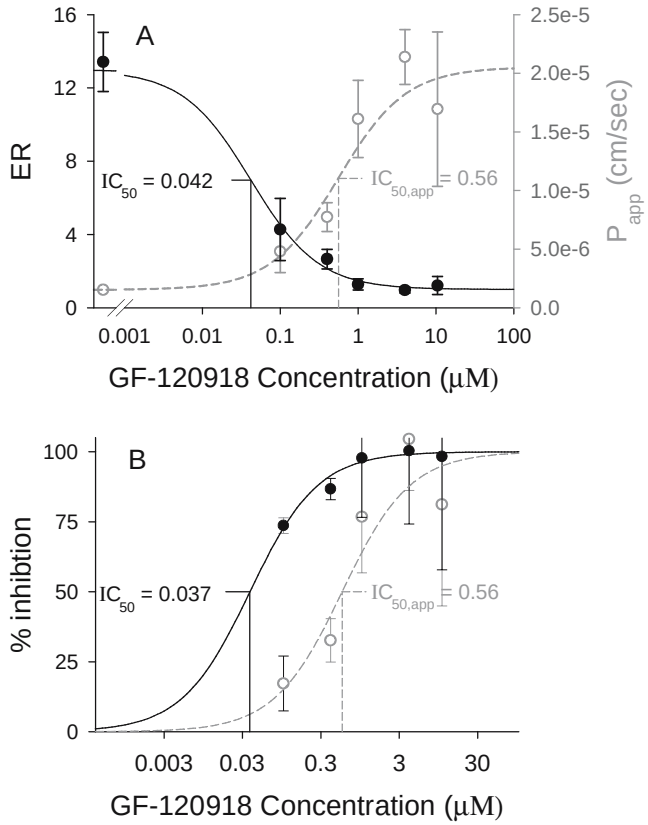

Fig. 4. Influence of GF-120918 on the brain uptake of quinidine. Data from Chen *et al.* (13). (A) *In situ* brain perfusion P_{app} and ER values for quinidine were determined in the presence of various concentrations of GF-120918 (*solid* and *open symbols*, respectively). Modified Michaelis–Menten equations $[PS = PS_0 + (PS_I - PS_0) \times \frac{[I]}{[I]+IC_{50,app}}$ or $ER = ER_{max} + (ER_{max} - 1) \times \frac{[I]}{[I]+IC_{50}}]$ were fit to the P_{app} or ER data to obtain estimates of $IC_{50,app}$ and IC_{50} respectively. (B) Inhibition of P-gp-mediated efflux was calculated from the P_{app} data using either Eq. (12–5), a commonly cited inhibition equation (*open symbols*), or Eq. (12–4), a newly derived inhibition equation (*solid symbols*), and the Michaelis–Menten equation was fitted to the inhibition data to obtain estimates of $IC_{50,app}$ and IC_{50}, respectively. Note that in both panels (A) and (B), $IC_{50,app}$ overestimated IC_{50}, and that $IC_{50,app} = ER_{max} \times IC_{50}$.

This phenomenon has been observed for other efflux substrates transported by multiple proteins, such as fexofenadine and digoxin (18,19). In cases in which active transport processes are present in addition to efflux, estimates of kinetic efflux parameters (IC_{50}, K_m, or PS_{efflux}) may be confounded by the action of the other transport process(es). Experimental determination of efflux transporter kinetic parameters is difficult when flux is influenced by multiple systems (i.e., active uptake and efflux), because inhibitors often are nonselective and the K_m(s) of additional active process(es) may be less than that of the efflux transporter.

Asymmetry and Basolateral Efflux Ratios are not Identical

The basolateral and asymmetry efflux ratios (ER_B and ER_α) are used to characterize the influence of efflux on a given model system and to extrapolate observations from one model system to another (i.e., *in vitro* to *in vivo* predictions). Thus, it is important to understand the relationship between ER_B and ER_α, which may be best understood by examining the relationship between ER_α-1 and ER_B-1 from rearrangement of Eqs. (7–3) and (6–3):

$$ER_\alpha - 1 = \left(\frac{PS_A + PS_{efflux}}{PS_A}\right) - 1 \qquad (11\text{–}1)$$

$$ER_B - 1 = \left(\frac{PS_A + PS_B + PS_{efflux}}{PS_A + PS_B}\right) - 1 \qquad (11\text{–}2)$$

If $PS_A = PS_B$, then the ratio of ER_α-1 and ER_B-1 equals 2 as shown in Eq. (11–3).

$$\frac{ER_\alpha - 1}{ER_B - 1} = \frac{\left(\frac{PS_A+PS_{efflux}}{PS_A}\right) - 1}{\left(\frac{PS_A+PS_B+PS_{efflux}}{PS_A+PS_B}\right) - 1} = 2 \qquad (11\text{–}3)$$

Equation (11–3) illustrates that ER_α is larger than ER_B and that, when PS_{efflux} is large compared to PS_A, ER_α will equal twice ER_B.

The fact that $ER_\alpha > ER_B$ may explain why the *in situ* brain perfusion P-gp efflux ratio underpredicts the *in vivo* brain-to-plasma efflux ratio. Several studies have examined the influence of P-gp on brain uptake of P-gp substrates, and developed relationships for the difference in brain uptake clearance (Cl_{up}) and brain-to-plasma ratio ($K_{p,brain}$) between P-gp-deficient and P-gp-competent mice. The *in situ* P-gp efflux ratio (9), which is analogous to ER_B and is determined by dividing Cl_{up} in P-gp-deficient mice ($Cl_{up}^{-/-}$) by the brain uptake clearance in P-gp-competent mice ($Cl_{up}^{+/+}$), has been used to predict the *in vivo* P-gp efflux ratio, which is calculated by dividing the $K_{p,brain}$ in P-gp-deficient mice ($K_{p,brain}^{-/-}$) by the $K_{p,brain}$ in P-gp-competent mice ($K_{p,brain}^{+/+}$). In most studies, the *in situ* efflux ratio correlated well with the *in vivo* efflux ratio, although the *in situ* efflux ratio consistently

Table IV. Influence of P-gp-Efflux on the Brain-to-Plasma Ratio ($K_{p,brain}$) and Brain Equilibration Rate Constant ($K_{brain,eq}$) of P-gp Substrates

	Actual fold change in $K_{p,brain}$ (ER_α)[a]	Actual fold change in $K_{brain,eq}$ (ER_A)[a]	Expected change in $K_{brain,eq}$ (ER_A)[b]
Fentanyl	1.9	1.0	1.3
Alfentanil	2.8	1.4	1.5
Methadone	7.2	2.4	1.8
Loperamide	44	1.9	2

[a] Unpublished experimental observations.
[b] The expected change in change in $K_{brain,eq}$ was calculated from the fold change in $K_{p,brain}$ and the theoretical relationship between ER_α and ER_A. $ER_A = 2ER_\alpha / (1+ER_\alpha)$.

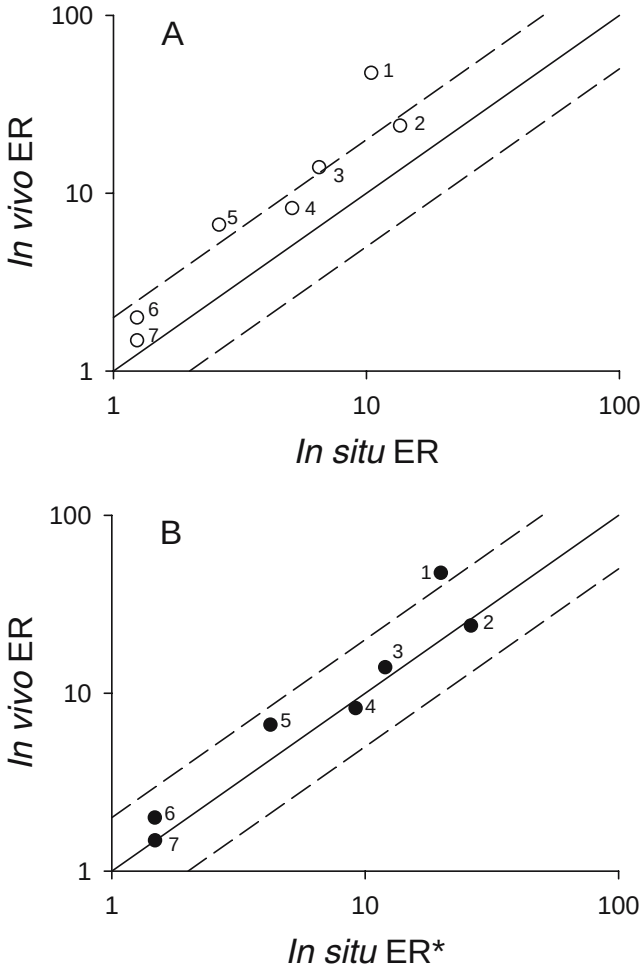

Fig. 5. Correlation between *in situ* and *in vivo* P-gp efflux ratios. (A) *In situ* efflux ratio was by defined as the ratio of brain uptake clearance in P-gp-deficient mice divided by the brain uptake clearance in P-gp-competent mice. *In vivo* efflux ratio was calculated as the brain-to-plasma ratio of P-gp-deficient mice divided by the brain-to-plasma ratio of P-gp-competent animals. In panel (B), *in situ* ER* was corrected for differences between ER_A and ER_α($ER^* = [(ER - 1) \times 2] + 1$). *Solid line* represents line of unity whereas *dashed lines* represent twofold above or below the line of unity. Compound legend is as follows: 1 loperamide, 2 quinidine, 3 ritonavir, 4 verapamil, 5 methadone, 6 fentanyl, 7 morphine.

underpredicted the *in vivo* efflux ratio [Fig. 5; data from references (9,11,20,21) and unpublished observations]. This underprediction is expected since the *in situ* P-gp efflux ratio is analogous to ER_B and the *in vivo* efflux ratio is analogous to ER_α. Direct predictions can be made by comparing the *in situ* efflux ratio minus one to the *in vivo* efflux ratio minus one. The *in situ* efflux ratio minus one is expected to equal one half the *in vivo* efflux ratio minus one. When the *in situ* and *in vivo* efflux ratios are compared in this manner, the *in situ* efflux ratio no longer underpredicts the *in vivo* efflux ratio (Fig. 5).

Apparent IC_{50} and K_m are Influenced by Efflux Activity

The efflux activity (PS_{efflux}) in the presence of efflux inhibition can be expressed as in Eq. (12–1), where $PS_{efflux,max}$ is the efflux activity in the absence of inhibition (i.e., when the efflux ratio equals ER_{max}), and ϕ_i is the degree of efflux inhibition:

$$PS_{efflux} = PS_{efflux,max} \times (1 - \phi_i) \tag{12–1}$$

As derived previously, the efflux activity (PS_{efflux}) is proportional to ER_α-1, ER_B-1 and $ER_{C(t\to\infty)}$-1. When ER-1 and ER_{max}-1 are substituted for PS_{efflux} and $PS_{efflux,max}$ respectively, then Eq. (12–1) can be rewritten as follows:

$$ER - 1 = (ER_{max} - 1) \times (1 - \phi_i) \tag{12–2}$$

Solving Eq. (12–2) for ϕ_i yields:

$$\phi_i = \frac{ER_{max} - ER}{ER_{max} - 1} \tag{12–3}$$

From this point forward, the symbol PS will represent any experimental variable that is attenuated by efflux in a manner consistent with the model in Fig. 1, such as $PS_{A\to B}$ (i.e., P_{app} or A-to-B flux), cellular partition ratio, or brain-to-plasma ratio. The efflux ratio (ER) can be defined as (PS_I/PS), where PS_I is the value of PS when efflux is inhibited completely. When efflux activity is completely inhibited, ER equals unity. In the absence of any efflux inhibition, ER equals ER_{max}, defined as (PS_I/PS_0), where PS_0 is the value of PS in the absence of efflux inhibition. Equation (12–3) can be expressed in terms of PS by substituting (PS_I/PS_0) and (PS_I/PS) for ER_{max} and ER.

$$\phi_i = \frac{PS_I}{PS} \times \frac{(PS - PS_0)}{(PS_I - PS_0)} \tag{12–4}$$

Equation (12–5) represents the standard equation used to calculate ϕ_i in the literature and it differs from Eq. (12–4) by a factor of PS_I/PS:

$$\phi_{i,app} = \frac{PS - PS_0}{PS_I - PS_0} \tag{12–5}$$

This difference between the kinetically derived Eq. (12–4) and Eq. (12–5) has a profound impact on calculating IC_{50}, K_m, and understanding the relationship between PS and ϕ_i (see Table III). Use of Eq. (12–5) does not yield true kinetic parameters for the system, but rather apparent parameters. This can be illustrated by solving Eqs. (12–4) and (12–5) for PS, yielding Eqs. (12–6) and (12–7), respectively:

$$PS = \frac{PS_I \times PS_0}{PS_I + (PS_0 - PS_I) \times \phi_i} \tag{12–6}$$

$$PS = PS_0 + (PS_I - PS_0) \times \phi_{i,app} \tag{12–7}$$

Examination of Eq. (12-7) reveals that the maximum increase in PS due to inhibition is PS_I-PS_0; when $\phi_{i,app}$ equals 50%, the increase in PS equals one half the maximum possible increase (i.e., the change in PS is directly proportional to $\phi_{i,app}$).

The actual fold change in PS due to efflux inhibition may be expressed in terms of efflux ratios or permeability-surface area products:

$$\text{fold}\,\Delta PS = \frac{PS}{PS_0} = \frac{PS_I/PS_0}{PS_I/PS} = \frac{ER_{max}}{ER} \tag{12–8}$$

Solving Eq. (12–3) for ER and substituting into Eq. (12–8) yields:

$$\text{fold}\,\Delta\,\text{PS} = \frac{\text{ER}_{\max}}{\text{ER}_{\max} - (\text{ER}_{\max} - 1) \times \phi_i} \tag{12–9}$$

Assuming $\phi_i = \frac{[I]}{[I]+IC_{50}}$, the maximum fold change in PS at any inhibitor concentration [I] is determined by the upper limits of Eq. (12–9):

$$\frac{[I]}{IC_{50}} + 1 \geq \text{fold}\,\Delta\,\text{PS} \leq \text{ER}_{\max} \tag{12–10}$$

According to the theoretically derived Eq. (12–10), at 50% inhibition ([I]=IC_{50}) the maximum increase in *PS* is twofold. This is contrary to the relationship in Eq. (12–7). However, it is analogous to the case in which 50% inhibition of a specific clearance pathway (i.e., CYP3A4) will result in at most a twofold increase in steady-state concentrations (22).

The difference between the theoretically derived Eq. (12–6) and the simple Eq. (12–7) can be illustrated further by comparing estimates of IC_{50} and K_m obtained from the two equations. The nonlinear relationships between PS and IC_{50} derived from the kinetic model in Fig. 1 can be expressed as in Eq. (12–11). Similarly, the relationship between PS and K_m can be expressed as in Eq. (12–12):

$$\text{PS} = \frac{\text{PS}_I \times \text{PS}_0}{\text{PS}_I + (\text{PS}_0 - \text{PS}_I) \times \frac{[I]}{[I]+IC_{50}}} \tag{12–11}$$

$$\text{PS} = \frac{\text{PS}_I \times \text{PS}_0}{\text{PS}_I + (\text{PS}_0 - \text{PS}_I) \times \frac{[S]}{[S]+K_m}} \tag{12–12}$$

Using the relationship in Eq. (12–7), PS can be expressed in terms of $IC_{50,app}$ or $K_{m,app}$ by substituting {[I]/([I]+$IC_{50,app}$)} or {[S]/([S]+$K_{m,app}$)} for $\phi_{i,app}$:

$$\text{PS} = \text{PS}_0 + (\text{PS}_I - \text{PS}_0) \times \frac{[I]}{[I] + IC_{50,app}} \tag{12–13}$$

$$\text{PS} = \text{PS}_0 + (\text{PS}_I - \text{PS}_0) \times \frac{[S]}{[S] + K_{m,app}} \tag{12–14}$$

Differences in $IC_{50,app}$ and $K_{m,app}$ calculated by standard equations in current use *vs.* those suggested herein can be illustrated by substituting PS from Eq. (12–11) into Eq. (12–13) and solving for $IC_{50,app}$ and by substituting PS from Eq. (12–12) into Eq. (12–14) and solving for $K_{m,app}$:

$$IC_{50,app} = IC_{50} \times \frac{\text{PS}_I}{\text{PS}_0} = IC_{50} \times \text{ER}_{\max} \tag{12–15}$$

$$K_{m,app} = K_m \times \frac{\text{PS}_I}{\text{PS}_0} = K_m \times \text{ER}_{\max} \tag{12–16}$$

As can be seen from Eqs. (12–15) and (12–16), current methods used for calculating $K_{m,app}$ or $IC_{50,app}$ will result in overestimation of these parameters by a factor of ER_{max} (Fig. 4).

This overestimation poses a number of potential problems. The ER_{max} for a given model system is dependent on both the efflux activity of the system and the test substrate. When ER_{max} is small, the relative error in $K_{m,app}$ or $IC_{50,app}$ calculated from current methods will be small. However, model systems with high efflux activity and substrates with large ER_{max} are precisely the model systems and substrates that are most sensitive for identifying efflux substrates and inhibitors. The $IC_{50,app}$ of inhibitors should be properly ranked-ordered if testing is conducted with a common probe substrate and in a model system with a consistent efflux activity. However, when inhibitors are tested against dissimilar substrates and in different model systems expressing different efflux activity, then $IC_{50,app}$ and rank ordering of $IC_{50,app}$ may not correspond to the real IC_{50} or even the actual rank order. Lastly, the $IC_{50,app}$ of the same inhibitor will differ between different substrates if the substrates have different ER_{max}. This behavior may confound results or be attributed incorrectly to inhibition at different binding sites on the efflux transporter for different substrates.

The situation in which $K_{m,app}$ is affected by ER_{max} can be demonstrated by a recently reported study examining the flux of taurocholate through apical sodium-dependent bile acid transporter (hASBT). In this study with transfected MDCK monolayers, the $K_{m,app}$ of taurocholate was shown to increased as a function of hASBT expression. This unexpected and novel observation was attributed to aqueous boundary layer effects (23). Alternatively, since transporter expression and PS_{efflux} are proportional, the observation is entirely consistent with the expected relationship between $K_{m,app}$ and transporter expression [Eq. (12–16)]. If the K_m been calculated in a manner consistent with the kinetic model in Fig. 1 [Eq. 12–12], it is likely that that the "true" K_m would have been shown to be independent of hASBT expression, as expected.

Inhibiting Active Efflux to Reverse MDR or Increase Drug Brain Penetration

Arbitrarily, reversal of multidrug resistance (MDR) can be defined as less than a twofold difference in intracellular drug concentrations between naïve cells and MDR cells. The change in PS necessary to reverse MDR then can be defined accordingly by:

$$\text{fold}\,\Delta\,\text{PS} \geq \frac{\text{ER}_{\max}}{2} \tag{13–1}$$

From Eqs. (13–1) and (12–9), the degree of inhibition required to reverse MDR can be solved as:

$$\phi_i \geq \frac{\text{ER}_{\max} - 2}{\text{ER}_{\max} - 1} \tag{13–2}$$

The degree of efflux inhibition needed to reverse MDR therefore is dependent on ER_{max}. The higher the degree of MDR resistance, the higher the requisite degree of inhibition to reverse MDR. The inhibitor concentration necessary to reverse MDR can be determined by solving Eq. (13–2) for [I], assuming $\phi_i = \frac{[I]}{[I]+K_i}$:

$$[I] \geq (\text{ER}_{\max} - 2)K_i \tag{13–3}$$

In Eqs. (13–2) or (13–3), all positive values ϕ_i or [I] indicate the degree of inhibition or the inhibitor concentration necessary to inhibit efflux such that there is less than a twofold difference in drug resistance between MDR cells and naïve cell lines.

The degree of efflux inhibition necessary to reverse multidrug resistance is not simply a function of inhibitor K_i but also is dependent on ER_{max}. As cells become more resistant due to higher expression of the efflux transporter, the ER_{max} will increase, which will necessitate greater inhibition and consequently higher inhibitor concentrations to reverse MDR. Treatment with an efflux inhibitor will not reverse MDR in all cells equally, and will be less effective in cells possessing the highest degree of MDR. This, in turn, will result in tumors becoming more resistant because the most resistant cells will have a survival advantage. The relationships in Eqs. (13–2) and (13–3) are also applicable to reversing efflux at the blood–brain barrier in order to increase drug delivery of efflux substrates to the brain; substrates with larger values of ER_{max} will require a higher degree of efflux inhibition and higher inhibitor concentrations to overcome efflux.

A relevant case study to illustrate this point comes from a clinical study in which the specific P-gp inhibitor tariquadar was shown to completely inhibit P-gp in T lymphocytes [using the fluorescent dye $DiOC_2$ (3) as a probe], but was ineffective at inhibiting P-gp at the blood-brain barrier (using the opioid loperamide as a probe) (24). On first consideration, such observations may seem unexpected, and therefore lead to complex hypotheses to rectify apparently anomalous results. However, these observations are not, in fact, inconsistent. The ER_{max} of $DiOC_2$ (3) in T lymphocytes is ~4 (25), while the ER_{max} of loperamide at the blood-brain barrier has been estimated in preclinical experiments to be ~65 (26). Based on Eqs. (13–2) and (13–3) and the difference in ER_{max} between $DiOC_2$ (3) and loperamide, it is not surprising that complete inhibition of P-gp was observed in T lymphocytes but not in the blood-brain barrier.

CONCLUSION

A set of equations, based on a simple three-compartment model, was derived to describe the theoretical relationships between PS_{efflux} and PS, ER, ϕ_i, IC_{50}, and K_m. The resulting relationships show that current mathematical treatment of efflux data is inconsistent with this model. In particular, these relationships mistakenly assume that PS_{efflux} is proportional to the attenuation or enhancement in PS, and that 50% inhibition of efflux activity will result in 50% of the maximum possible change in PS. The theoretical relationships derived herein indicate that such an assumption will lead to an overestimate of ϕ_i, K_m and IC_{50} in proportion to the ER_{max} of the experimental system. These relationships also show that PS_{efflux} is proportional to the passive permeability multiplied by ER-1, and that 50% inhibition of efflux activity will result in at most a twofold increase in PS. In addition, apical efflux has a minimum impact on the B-to-A flux ($\leq$twofold), and consequently B-to-A efflux studies are insensitive approaches for estimating efflux kinetic parameters. Finally, the three-compartment model and kinetic considerations indicate that a larger degree of efflux inhibition is necessary to reverse the effects of efflux when the efflux ratio is large. Viewing efflux activity in terms of efflux ratios rather than change in PS allows for better conceptual understanding and more accurate estimation of kinetic parameters; therefore, it is recommended that efflux ratio be calculated and used when evaluating efflux activity and estimating the degree of efflux inhibition, IC_{50}, or K_m.

ACKNOWLEDGMENTS

We gratefully thank Maciej Zamek-Gliszczynski, Rong Zhao, and Beverly Mowrey for critically reading the manuscript. This work was supported by NIH GM61191 and Pfizer Inc. J. Cory Kalvass was supported by a predoctoral fellowship in pharmacokinetics and drug disposition from the Eli Lilly and Company Foundation.

REFERENCES

1. C. J. Matheny, M. W. Lamb, K. L. R. Brouwer, and G. M. Pollack. Pharmacokinetic and pharmacodynamic implications of P-glycoprotein modulation. *Pharmacotherapy*, **21**:778–796 (2001).
2. C. M. Kruijtzer, J. H. Beijnen, H. Rosing, W. W. ten Bokkel Huinink, M. Schot, R. C. Jewell, E. M. Paul, and J. H. Schellens. Increased oral bioavailability of topotecan in combination with the breast cancer resistance protein and P-glycoprotein inhibitor GF120918. *J. Clin. Oncol.* **20**:2943–2950 (2002).
3. H. Thomasand and H. M. Coley. Overcoming multidrug resistance in cancer: an update on the clinical strategy of inhibiting p-glycoprotein. *Cancer Control* **10**:159–165 (2003).
4. E. M. Kemper, C. Cleypool, W. Boogerd, J. H. Beijnen, and O. van Tellingen. The influence of the P-glycoprotein inhibitor zosuquidar trihydrochloride (LY335979) on the brain penetration of paclitaxel in mice. *Cancer Chemother. Pharmacol.* **53**:173–178 (2004).
5. R. H. Ho and R. B. Kim. Transporters and drug therapy: implications for drug disposition and disease. *Clin. Pharmacol. Ther.* **78**:260–277 (2005).
6. J. H. Lin. Drug–drug interaction mediated by inhibition and induction of P-glycoprotein. *Adv. Drug Deliv. Rev.* **55**:53–81 (2003).
7. A. J. Sadeque, C. Wandel, H. He, S. Shah, and A. J. Wood. Increased drug delivery to the brain by P-glycoprotein inhibition. *Clin. Pharmacol. Ther.* **68**:231–237 (2000).
8. Y. Adachi, H. Suzuki, and Y. Sugiyama. Comparative studies on in vitro methods for evaluating in vivo function of MDR1 P-glycoprotein. *Pharm. Res.* **18**:1660–1668 (2001).
9. C. Dagenais, J. Zong, J. Ducharme, and G. M. Pollack. Effect of mdr1a P-glycoprotein gene disruption, gender, and substrate concentration on brain uptake of selected compounds. *Pharm. Res.* **18**:957–963 (2001).
10. C. Chen, X. Liu, and B. J. Smith. Utility of Mdr1-gene deficient mice in assessing the impact of P-glyco-protein on pharmacokinetics and pharmacodynamics in drug discovery and development. *Curr. Drug Metab.* **4**:272–291 (2003).
11. M. Yamazaki, W. E. Neway, T. Ohe, I. Chen, J. F. Rowe, J. H. Hochman, M. Chiba, and J. H. Lin. In vitro substrate identification studies for p-glycoprotein-mediated transport: species difference and predictability of in vivo results. *J. Pharmacol. Exp. Ther.* **296**:723–735 (2001).
12. T. T. Tran, A. Mittal, T. Aldinger, J. W. Polli, A. Ayrton, H. Ellens, and J. Bentz. The elementary mass action rate constants of P-gp transport for a confluent monolayer of MDCKII-hMDR1 cells. *Biophys. J.* **88**:715–738 (2005).
13. J. Bentz, T. T. Tran, J. W. Polli, A. Ayrton, and H. Ellens. The steady-state Michaelis–Menten analysis of P-glycoprotein mediated transport through a confluent cell monolayer cannot predict the correct Michaelis constant Km. *Pharm. Res.* **22**:1667–1677 (2005).
14. H. Kwon, R. A. Lionberger, and L. X. Yu. Impact of P-glycoprotein-mediated intestinal efflux kinetics on oral bioavailability of P-glycoprotein substrates. *Mol. Pharm.* **1**:455–465 (2004).
15. W. Chen, J. Z. Yang, R. Andersen, L. H. Nielsen, and R. T. Borchardt. Evaluation of the permeation characteristics of a model opioid peptide, H-Tyr-D-Ala-Gly-Phe-D-Leu-OH

(DADLE), and its cyclic prodrugs across the blood–brain barrier using an in situ perfused rat brain model. *J. Pharmacol. Exp. Ther.* **303**:849–857 (2002).
16. K. M. Mahar Doan, J. E. Humphreys, L. O. Webster, S. A. Wring, L. J. Shampine, C. J. Serabjit-Singh, K. K. Adkison, and J. W. Polli. Passive permeability and P-glycoprotein-mediated efflux differentiate central nervous system (CNS) and non-CNS marketed drugs. *J. Pharmacol. Exp. Ther.* **303**:1029–1037 (2002).
17. M. D. Troutman, and D. R. Thakker. Rhodamine 123 requires carrier-mediated influx for its activity as a P-glycoprotein substrate in Caco-2 cells. *Pharm. Res.* **20**:1192–1199 (2003).
18. N. Petri, C. Tannergren, D. Rungstad, and H. Lennernas. Transport characteristics of fexofenadine in the Caco-2 cell model. *Pharm. Res.* **21**:1398–1404 (2004).
19. M. E. Taub, L. Podila, D. Ely, and I. Almeida. Functional assessment of multiple P-glycoprotein (P-gp) probe substrates: influence of cell line and modulator concentration on P-gp activity. Drug Metab. Dispos. **33**:1679–1687 (2005).
20. C. Dagenais, C. L. Graff, and G. M. Pollack. Variable modulation of opioid brain uptake by P-glycoprotein in mice. *Biochem. Pharmacol.* **67**:269–276 (2004).
21. H. Kusuhara and Y. Sugiyama. Efflux transport systems for drugs at the blood-brain barrier and blood-cerebrospinal fluid barrier (Pt. 2). *Drug Discov. Today* **6**:206–212 (2001).
22. M. Rowland and S. B. Matin. Kinetics of drug–drug interactions. *J. Pharmacokinet. Biopharm.* **1**:553–567 (1973).
23. A. Balakrishnam and J. E. Polli. Bias in estimation of transporter kinetic parameters: interplay of transporter expression level and substrate affinity. *J. Clin. Pharmacol.* **45**:1087 (2005).
24. M. Muszkat, D. Kurnik, G. G. Sofowora, J. P. Donahue, G. R. Wilkinson, and A. J. Wood. Tariquidar (TAR, XR-9576) selectively inhibits P-glycoprotein (P-GP) in T-lymphocytes compared to that in the blood–brain barrier (BBB). *Clin. Pharmacol. Ther.* **77**:39 (2005).
25. T. Hulgan, J. P. Donahue, C. Hawkins, D. Unutmaz, R. T. D'Aquila, S. Raffanti, F. Nicotera, P. Rebeiro, H. Erdem, M. Rueff, and D. W. Haas. Implications of T-cell P-glycoprotein activity during HIV-1 infection and its therapy. *J. Acquir. Immune Defic. Syndr.* **34**:119–126 (2003).
26. J. C. Kalvass, C. L. Graff, and G. M. Pollack. Use of loperamide as a phenotypic probe of mdr1a status in CF-1 mice. *Pharm. Res.* **21**:1867–1870 (2004).
27. K. Yasuda, L. B. Lan, D. Sanglard, K. Furuya, J. D. Schuetz, and E. G. Schuetz. Interaction of cytochrome P450 3A inhibitors with P-glycoprotein. *J. Pharmacol. Exp. Ther.* **303**:323–332 (2002).
28. B. Bauer, D. S. Miller, and G. Fricker. Compound profiling for P-glycoprotein at the blood–brain barrier using a microplate screening system. *Pharm. Res.* **20**:1170–1176 (2003).
29. M. Barecki-Roach, E. J. Wang, and W. W. Johnson. Many P-glycoprotein substrates do not inhibit the transport process across cell membranes. *Xenobiotica* **33**:131–140 (2003).
30. J. Zong and G. M. Pollack. Modulation of P-glycoprotein transport activity in the mouse blood–brain barrier by rifampin. *J. Pharmacol. Exp. Ther.* **306**:556–562 (2003).
31. C. Wandel, R. Kim, M. Wood, and A. Wood. Interaction of morphine, fentanyl, sufentanil, alfentanil, and loperamide with the efflux drug transporter P-glycoprotein. *Anesthesiology* **96**:913–920 (2002).